Environmental Science & Technology

ARTICLE

pubs.acs.org/est

Process-Based Reactive Transport Model To Quantify Arsenic Mobility during Aquifer Storage and Recovery of Potable Water

Ilka Wallis,*[,†] Henning Prommer,[‡,§,⊥] Thomas Pichler,[∥] Vincent Post,[†,⊥] Stuart B. Norton,[#] Michael D. Annable,[#] and Craig T. Simmons[†,⊥]

[†]School of the Environment, Flinders University, Adelaide, GPO Box 2100, SA 5001, Australia

[‡]CSIRO Land and Water, Private Bag No. 5, Wembley WA 6913, Australia

[§]School of Earth and Environment, The University of Western Australia, Crawley 6009, Australia

[∥]Department of Geosciences, University of Bremen, 28334 Bremen, Germany

[⊥]National Centre for Groundwater Research and Training, Flinders University, Adelaide, GPO Box 2100, SA 5001, Australia

[#]Department of Environmental Engineering Sciences, University of Florida, Florida 32611-2013, United States

Supporting Information

ABSTRACT: Aquifer storage and recovery (ASR) is an aquifer recharge technique in which water is injected in an aquifer during periods of surplus and withdrawn from the same well during periods of deficit. It is a critical component of the long-term water supply plan in various regions, including Florida, USA. Here, the viability of ASR as a safe and cost-effective water resource is currently being tested at a number of sites due to elevated arsenic concentrations detected during groundwater recovery. In this study, we developed a process-based reactive transport model of the coupled physical and geochemical mechanisms controlling the fate of arsenic during ASR. We analyzed multicycle hydrochemical data from a well-documented affected southwest Floridan site and evaluated a conceptual/numerical model in which (i) arsenic is initially released during pyrite oxidation triggered by the injection of oxygenated water (ii) then largely complexes to neo-formed hydrous ferric oxides before (iii) being remobilized during recovery as a result of both dissolution of hydrous ferric oxides and displacement from sorption sites by competing anions.

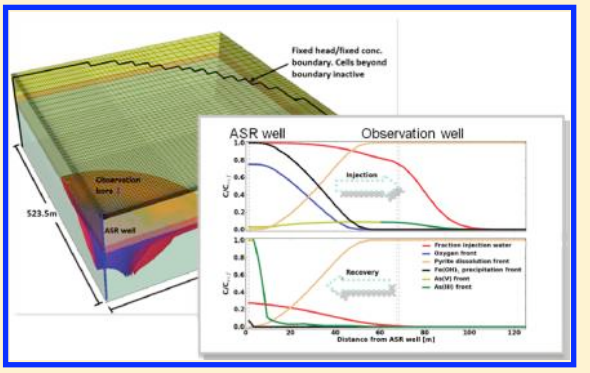

INTRODUCTION

Aquifer storage and recovery (ASR) is an aquifer recharge technique in which potable, reclaimed, or other water sources are injected into aquifers during periods of surplus and withdrawn from the same well during periods of deficit. In cases where oxic water is recharged into reducing aquifers, however, mobilization of trace metals may occur as a result of the oxidation of iron-sulfides or other reductants.

The interest in ASR as a critical component of long-term water supply strategies has increased in recent years. For example in Florida there are more than 50 ASR facilities in operation or permitted for construction[1] to compensate for seasonal imbalances between water supply and demand. Typically, these ASR operations involve the periodic injection of oxygenated water into the anoxic upper Floridan Aquifer System (FAS) and its later withdrawal. The viability of ASR as a safe and cost-effective water resource is currently being tested due to elevated arsenic (As) concentrations found at many sites.[2] While in general, neither the injected water nor the native groundwater has any appreciable concentrations of As, concentrations in the recovered water are reported to be elevated, often above the U.S. drinking water standard of 10 μg L^{-1}.[3]

A range of conceptual/numerical models for arsenic release and attenuation during ASR or similar push−pull operations were previously proposed. For example Appelo and de Vet[4] reported elevated As concentrations during *in situ* iron removal operations in The Netherlands, where oxygenated water was recharged into an anoxic siliclastic aquifer. The results of their geochemical modeling suggested that at their site competitive displacement of As by native groundwater containing phosphate was the most likely As release mechanism during the recovery phases. The same mechanism was suggested by Vanderzalm et al.[5] for an ASR site in Australia where reclaimed water was injected into a reducing carbonate aquifer. Studies by Stuyfzand and Timmer[6] and Wallis et al.[7] investigated elevated As concentrations at an aquifer storage transfer and recovery (ASTR) site in a siliclastic aquifer. Here, As release was closely associated with the oxidation of pyrite upon injection of oxygenated water. Under the progressively expanding oxic conditions, ferrous iron

Received: April 15, 2011
Accepted: July 1, 2011
Revised: June 30, 2011
Published: July 01, 2011

released during pyrite dissolution oxidized and precipitated as hydrous ferric oxides (HFO), thereby providing a successively increasing number of sorption sites for As. This was thought to be the key attenuation mechanism that caused elevated As concentrations to diminish to background concentrations after an initial period of elevated As concentrations close to the injection well.

For the aquifers selected by ASR operations in Florida, mineralogical and geochemical studies by Price and Pichler[8] and Jones and Pichler,[9] also suggested As-bearing pyrite to be the most likely source of As and sorption to neo-precipitated HFO to be the most likely arsenic attenuation mechanism during injection. However, the reversal of flow during the recovery phase causes a reversal to anoxic conditions that is thought to be responsible for the observed remobilization of arsenic.[2,10,11] Several alternative or complementary processes explaining this remobilization have been postulated. Mirecki[10] suggested the liberation of As to be associated with reductive dissolution of neo-precipitated HFO under sulfate-reducing conditions and the associated destruction of sorption sites. The instability of HFO during recovery was supported by inverse geochemical modeling. However, the calculated mass of HFO was minor, questioning the capacity of the aquifer material to effectively sorb and release the arsenic concentrations measured during cycle testing.[10] It was also speculated that arsenate may transform into arsenite under the reducing conditions, thus enhancing arsenic mobility due to diminished sorption affinity of As(III) on aquifer material compared to As(V). Stuyfzand[2] suggested the displacement of sorbed As by competing anions as a possible additional release mechanism.

For future design and operation of efficient and sustainable ASR facilities it is essential to have a clear understanding of the fundamental geochemical processes that control the mobility of As during ASR operations. In this study our aim was (i) to develop a numerical model that provides a process-based description of the physical and geochemical processes controlling the fate of arsenic during ASR and (ii) to test it for a comprehensive long-term field data set collected at an affected site in Florida.

MATERIALS AND METHODS

Field Site Used for Model Evaluation. Among the ASR sites reporting elevated As concentrations in the recovered water, the City of Bradenton ASR facility in southwest Florida was selected to evaluate the proposed model, because it offers a comparably comprehensive geochemical database and a well-defined site hydrogeology that is underpinned by geological and geophysical logs. The storage zone at the site is the Suwannee Limestone of the Upper Floridan Aquifer. The Suwannee Limestone is comprised primarily of carbonates, which contain clays intermixed with limestones near the formation top, and a thin layer of dolostone in the lower third.[12] Minor amounts of clay minerals and organic material, and trace amounts of quartz, gypsum, and pyrite are present.[12] Pyrite is ubiquitous throughout the Suwannee Limestone but is most abundant in high porosity zones and is generally As-rich with concentrations between 100 and 11200 ppm (average: 2300 ppm), while iron-oxides are absent.[8] The ASR storage zone at the site is confined and separated from the overlying superficial aquifer by interbedded carbonates, sands, and clays of the Hawthorn Group and overlies the chalky, fine- to coarse-grained Ocala Limestone. Based on flow meter measurements, it can be assumed that the ASR storage zone at the study site is relatively homogeneous except for a distinctly more permeable horizon at ~18 m below the top of the Suwannee Limestone.[11] The Bradenton ASR system consists of a single ASR well, and an observation well located at a distance of 68 m (Figure S1). Seven ASR cycles were conducted since construction of the site in November 2003. The cycles varied considerably both in timing and duration of the injection, storage, and recovery phases (Figure S2). They were documented by a monitoring program, as required by the Florida Department of Environmental Protection (FDEP) and water analysis followed the FDEP directions. The data are available from the FDEP (http://www.dep.state.fl.us/).

Numerical Model Approach and Model Setup. From the hydrogeological site characterization and the records of observed hydrochemical changes during the Bradenton ASR operation, conceptual models for (i) the physical processes (flow and nonreactive transport) and (ii) the geochemical processes were formulated. They were implemented numerically using the USGS code MODFLOW in conjunction with the reactive multicomponent transport code PHT3D.[13,14]

As (i) the native groundwater flow velocities are negligible compared to those induced by the ASR operation and (ii) the aquifer is expected to be homogeneous in lateral direction, the flow and transport conditions at the site were assumed to be radial-symmetric. In a first step, radial flow and nonreactive transport were simulated using a three-dimensional (3D) groundwater flow model that represents one-quarter of a radial-symmetric domain (Figure S1). The 3D model has a lateral extension of 523.5 m in both x and y directions, selected such that boundaries were sufficiently far from the ASR well to not impact solute concentration fronts during the simulated ASR cycles. The Suwannee Limestone section targeted by the ASR operation (ca. 120−180 m below ground level) was separated into 7 layers (Figure S1). The hydrogeological model and initial parameter estimates were based on geophysical log data and sedimentological characteristics of the aquifer [11] (Table 1). The flow model was run for a simulation period of 1176 days, commencing with the start of the first ASR cycle, and, therefore, native aquifer conditions. To represent the different phases of the ASR operation (i.e., storage, recharge and abstraction periods) the simulation time was discretized into 28 hydraulically and/or hydrochemically differing stress periods that varied in length between 5 and 423 days (Figure S2). Based on this flow model, a nonreactive transport model was set up and successively improved. Sulfate was selected as the key species to identify and constrain physical transport processes. Using sulfate as a (pseudo-) conservative species was justified in this specific case because concentrations in the injectate are only approximately 20% of the native groundwater concentration and the impact of pyrite oxidation on sulfate concentration is minimal due to the high native concentrations (Figure S3). In contrast, differences in chloride concentration between the injectate and the groundwater were negligible, and therefore chloride was found not to be a suitable tracer. The calibrated nonreactive model (Table 1) formed the basis for the subsequent reactive transport simulations. In order to reduce model execution times for the reactive transport simulations the 3D model was translated into a simpler two-dimensional quasi-radial flow/transport model (Figure S4). Because the simulation of radial flow is not an explicit feature of the flow simulator MODFLOW, the radially decreasing flow velocities were obtained by a variable layer thickness that corresponds to the perimeter at the radial distance of the grid-cell

Table 1. Calibrated Values of Adjustable Flow and Reaction Model Parameters and Parameter Values Reported in the Literature

parameter	unit	value	literature values	source[a]
		Flow Model		
hydraulic conductivity	[m d^{-1}]	4.75 (layer 1−2) 35 (layer 3−5) 1.6 (layer 6−7)	0.98−30	(1), (2)
longitudinal dispersivity	[m]	1	-	model calibration
vert./long. dispersivity ratio	-	0.1	-	model calibration
effective porosity	-	0.2	0.19	(3)
		Reactive Transport Model		
sorption site density on HFO: (1) weak sites (2) strong sites	[mol/mol HFO]	(1) 0.06 (2) 0.0015	(1) 0.2−0.066 (2) 0.005−0.00165	(4), (5)
pyrite concentration (aquifer average)	[mg/kg]	819	276−32406	(6)
As in pyrite	[wt%]	0.5	0.01−1.12	(6)

[a] References: (1): Norton (2007); (2) Pyne (2007); (3) Stuyfzand (2008), (4) Dzombak and Morel (1990); (5) Appelo et al. (1999); (6) Price and Pichler (2006).

center, i.e., the distance from the ASR well, as discussed earlier by Greskowiak et al.[15]

Hydrogeochemical Characteristics, Conceptual Model, and Selected Reaction Network. The ASR operation involved the cyclic injection of oxygenated water into the reduced Suwannee Limestone aquifer. The native groundwater was clearly anoxic, as indicated by the presence of sulfide at low concentrations ($\sim 1.8 \times 10^{-2}$ mmol L^{-1}). Its total dissolved arsenic concentrations (measured by ICP-MS) were below detection limit (DL) (DL varied between 1.3×10^{-6} and 3.7×10^{-5} mmol L^{-1}) (Table 2). Concentrations of calcium (5.1 mmol L^{-1}) and bicarbonate (2.1 mmol L^{-1}) indicated mineral equilibrium with the limestone ($SI_{Calcite}$ 0.06), and the pH was found to range between 7.2 and 7.3. The injectate was sourced from surface water and pretreated to potable quality. The chemical composition of the injectate differed clearly from the native groundwater and generally had an oxic character with dissolved oxygen concentrations varying between 0.23 and 0.34 mmol L^{-1}. NO_3 as a possible additional oxidant in the injectant water was not determined. The As concentrations in the recovered water exceeded the U.S. drinking water standard of 10 μg L^{-1} (1.3×10^{-4}mmol L^{-1}) in most cycles with maximum concentrations reaching 1.0×10^{-3} mmol L^{-1} (75 μg L^{-1}).

Three different mechanisms of arsenic release were thought to be operative. First, during injection, under progressively more oxidizing conditions, As-rich pyrite becomes unstable and releases arsenic and potentially other trace metals. Simultaneously; ferrous iron released during pyrite oxidation is oxidized and precipitates as HFO, providing sorption sites for arsenic.

Second, during recovery, when high TDS, reducing native groundwater passes back toward the ASR well, competition between As and other anions for the finite number of sorption sites on HFO releases As by desorption. Finally, the third release mechanism is the reductive dissolution of HFO under the progressively more reducing redox conditions. Potential reductants of iron oxides are hydrogen sulfide as well as dissolved organic carbon (DOC). However, the latter, where present, was thought to be largely recalcitrant given that despite the presence of sulfate in the ambient water, neither sulfate reduction nor an increase in TIC over time can be observed. Also, measured TOC concentrations during recovery were similar to the concentrations measured in the injectant (average of 0.22 mmol L^{-1} and 0.27 mmol L^{-1}, respectively). Thus, water-sediment interactions were considered to be the key reactions affecting water chemistry evolution at the Bradenton site, while homogeneous reactions, as they could occur for example in the presence of labile DOC, were assumed to be of minor importance. Based on this hypothesized conceptual model derived from the hydrochemical monitoring results and the geochemical characterization of the Suwannee Limestone,[8] a corresponding reaction network of mixed equilibrium and kinetic reactions was formulated.

Mineral Reactions. The mineral assemblage considered in the reactive transport simulations included calcite ($CaCO_3$), siderite ($FeCO_3$), pyrite (FeS_2), and amorphous HFO ($Fe(OH)_3$), based on the results of sediment analysis,[8] and on calculated saturation indices of the native water. Pyrite oxidation by oxygen was modeled as a kinetic reaction following Williamson and Rimstidt,[16] while all other minerals were included as equilibrium reactions (thermodynamic data taken from the PHREEQC standard database). The release of As was stochiometrically linked to pyrite oxidation, as described in refs 7 and 17 with the molar ratio of As to FeS_2 based on data by Price and Pichler [8] (Figure S5, Table 1).

Surface Complexation and Ion Exchange Reactions. The dynamic changes in the sorption capacity that result from the precipitation and dissolution of HFO play a key role in explaining the observed As behavior. This process was modeled by coupling the moles of the surface complex sites to the mass of HFO in the aquifer.[7] The database of Dzombak and Morel[18] for sorption on HFO was employed, extended by reactions for Fe^{2+} and HCO_3^- [19] to allow for competition of inorganic solute species for the sorption sites provided by HFO. The properties of HFO were defined according to the values proposed by Dzombak and Morel.[18] However, the amount of sorption sites on HFO in the sediment is not known, and it is probably not identical for amorphous oxides and more crystalline aged oxides.[20] The number of sorption sites on HFO was therefore used as a fitting parameter. In addition, one cation exchanger site was included to account for the exchange of cations and hydrogen on clay surfaces.

Reaction Parameter Calibration. The selected reaction network was kept as simple as possible and was mainly based on equilibrium reactions. Thus, the model only includes a limited

Table 2. Measured and Modeled Injectant and Initial (i.e., Native Groundwater) Concentrations of Aqueous Components, Minerals, and Exchanger Composition

	measured concentration [mmol L^{-1}][a]		equilibrated and charge balanced initial model concentration [mmol L^{-1}][a]	
	native groundwater[b]	injectant[c]	native groundwater	injectant
		Aqueous Components		
pH	7.2−7.3	7.3−7.9	7.3	7.7
pe	-	-	−3.7	13.0
C(4)	2.0−2.1[d]	0.97−1.2[d]	2.38	1.04
C(−4)	-	-	7.8×10^{-6}	0.0
Ca	4.3−5.5	1.0−1.5	5.24	1.1
Na	1.0−1.1	2.0−2.3	1.09	2.0
Cl	0.93−1.3	0.73−1.0	1.00	0.91
Fe(2)	$<2 \times 10^{-4}$−$<5.2 \times 10^{-4}$	$<2 \times 10^{-4}$−$<5.2 \times 10^{-4}$	0.0	0.0
Fe(3)	-	-	0.0	0.0
K[e]	0.09−0.1	0.049	0.098	0.049
Mg	2.8−3.3	0.33−0.63	3.2	0.354
O(0)	3.1×10^{-4}−3.8×10^{-3}	0.23−0.34	0.0	0.25−0.36
S(6)	6.5−7.5	1.5−2.1	7.4	1.56
S(−2)	$<1 \times 10^{-2}$−4.7×10^{-2}	$<1 \times 10^{-2}$	1.8×10^{-2}	0.0
As	$<4 \times 10^{-5}$	$<4 \times 10^{-5}$	0	0
Tmp.	26.0−26.7	17.1−29.8	26.0	22.4
Initial Exchanger Composition (Model)				
CaX2	18.1			
MgX2	6.6			
NaX	0.29			
KX	0.13			
FeX2	0.0			
Initial Mineral Concentrations (Model)				
pyrite (FeS_2)	0.000175 (layer 1−2)			
	0.016 (layer 3−5)			
	0.018 (layer 6−7)			
calcite ($CaCO_3$)	0.53			
ferrihydrite ($Fe(OH)_3$)	0.0			
siderite ($FeCO_3$)	0.0			

[a] Except temperature in [°C], minerals in [mol L^{-1} of bulk aquifer volume] and pH, pe. [b] Measured at observation well SZMW-1 at the end of abstraction, where abstraction volume > injection volume. [c] Measured at ASR well at the end of injection periods. [d] HCO_3^-. [e] K data from Jones and Pichler (2007).

number of adjustable parameters (Table 1). These include the stoichiometric ratio of As within pyrite, the initial concentrations of pyrite in the aquifer matrix, and the sorption site density of HFO. Matching simulated and measured oxygen, ferrous iron and total As concentrations served as the main constraint for the estimation of these parameters. In the case of the initial pyrite concentration and the As-FeS_2 stoichiometric ratio trialed values were kept within the range reported by Price and Pichler[8] (Figure S5, Table 1).

Native Groundwater, Injectate, and Aquifer Matrix Composition. The physicochemical composition of the waters was based on the data published by the FDEP. The reported analyses were obtained during cycle tests primarily to assess ASR system performance and to ensure that recovered water meets state and federal drinking-water-quality criteria.[11] The Bradenton site geochemical data set was comprehensive in comparison to other ASR facilities in southwest Florida but still exhibited data gaps. For example, not all major and minor ions were consistently analyzed, and sampling frequencies differed between the ASR and observation well. Thus, native groundwater chemistry was inferred from the water composition measured at the monitoring well at the end of prolonged extraction periods (abstracted volumes ≥ injected volumes), when the measured concentrations indicated convergence toward a constant water quality. The modeled injectate water composition was generally based on the average of the water compositions measured at the ASR well during injection, although the documented variability of the oxygen concentrations in the injectate was considered. Water compositions were charge-balanced with PHREEQC-2 by adjusting the chloride concentration. The measured and model input concentrations of the native water and injectate together with initial mineral and exchanger compositions are listed in Table 2.

RESULTS AND DISCUSSION

Conservative Transport Behavior. The clear contrast between higher native and lower injectate sulfate concentrations

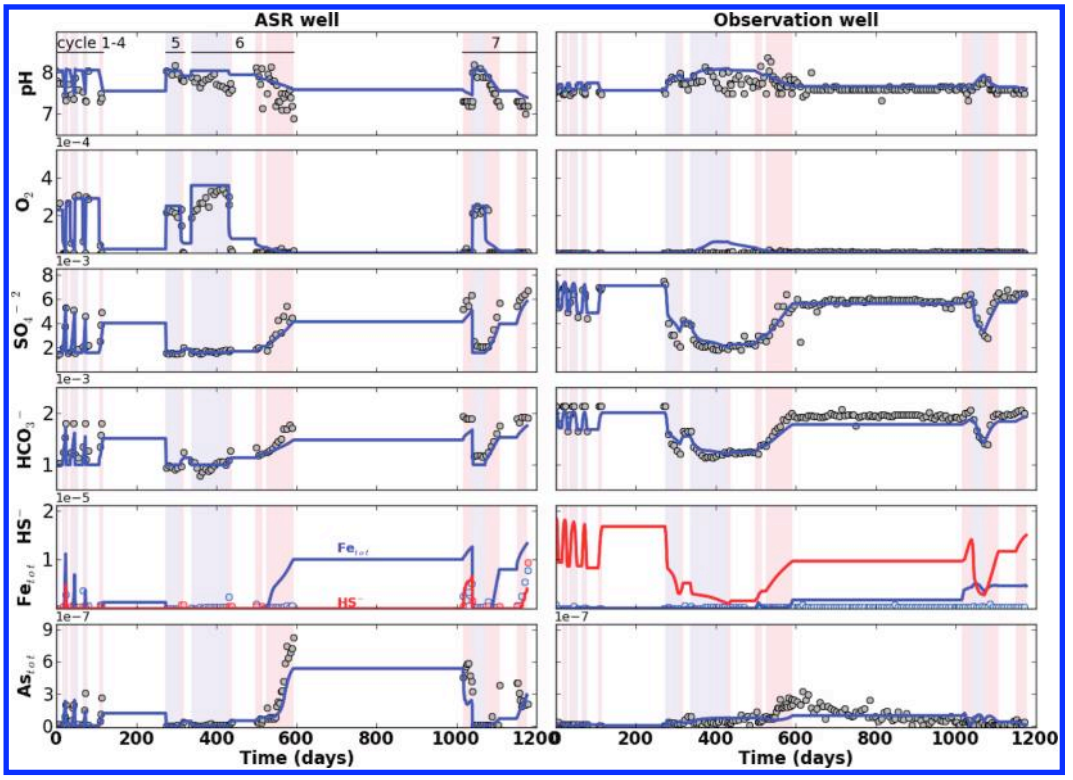

Figure 1. Measured (circles) and simulated (solid lines) aqueous concentrations of pH and selected ions for the 7 simulated ASR cycles. Injection periods are marked in light blue, recovery phases in light red, and intercycle storage periods in white. Concentrations are in mol L^{-1}, except pH.

was used to constrain the flow and physical transport behavior. Hydraulic conductivities as well as longitudinal and vertical dispersivities were adjusted until the simulated sulfate breakthrough curves fitted the corresponding observation data from both the ASR and the observation well (Table 1). In the calibrated model the simulated dynamic concentration changes are in good agreement with the measured data (Figure 1), including the rapid breakthrough of low sulfate water at the observation well. This rapid breakthrough is a result of the high permeability horizon that is present in the storage zone (35 m/d, model layers 3 to 5). In the calibrated model ~55% of the injected water penetrates through this section of the aquifer, and accordingly the injectant plume front moves faster through this horizon during injection and recovery. The penetration distances of the plume (50% of ΔSO_4) during the longest injection cycle (cycle 6) is ~240 m within the high conductivity horizon, while it is only ~120 m and ~70 m in the lower conductivity horizons above and below this zone, respectively. During the first four ASR cycles, all of which had similar injection/abstraction volumes, a freshening of the storage zone is evident from the successively lower measured and modeled sulfate concentrations at the observation well during injection.

Redox Zonation. The model simulations illustrate how aerobic water penetrated into the aquifer during the injection phase, thereby displacing the reducing native groundwater. With time pyrite oxidation consumed the oxygen of the injectate and caused the release of ferrous iron, which was subsequently oxidized and precipitated as HFO (Figure 2). The oxygen consumption rates and the resulting redox zonation varied as a result of the physical and chemical heterogeneity of the aquifer, i.e., the variability of the hydraulic conductivity and the estimated initial pyrite content. During the first five ASR cycles no oxygen breakthrough

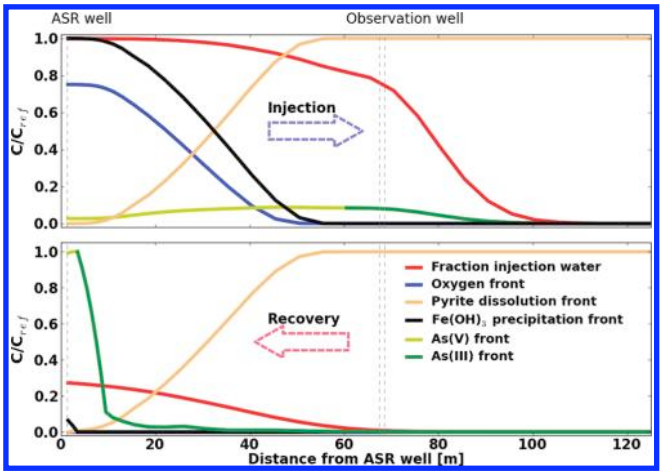

Figure 2. Concentration fronts of oxygen, As(III) and As(V), $Fe(OH)_3$ and extent of injected water (SO_4^{2-}) and pyrite dissolution during ASR cycle 1; a) at the end of injection and b) at the end of abstraction in the high permeability horizon (model layer 4). C_{ref} = reference concentration. For concentration O_2, SO_4^{2-}: C_{ref} = injectant concentration; for As, $Fe(OH)_3$, ΔC pyrite: maximum concentration during ASR cycle 1.

occurred at the observation well, as shown by both measurements and simulations (Figure 1). However, during cycle 6, where injection continued for several months (total injected volume = 453×10^6 L) model simulations showed the breakthrough of low concentrations of oxygen (5.8×10^{-2} mmol L^{-1}). While oxygen breakthrough at the observation well was not detected, the simulated breakthrough corresponds with a distinct increase in measured oxidation reduction potential (ORP) of up to 100 mV,

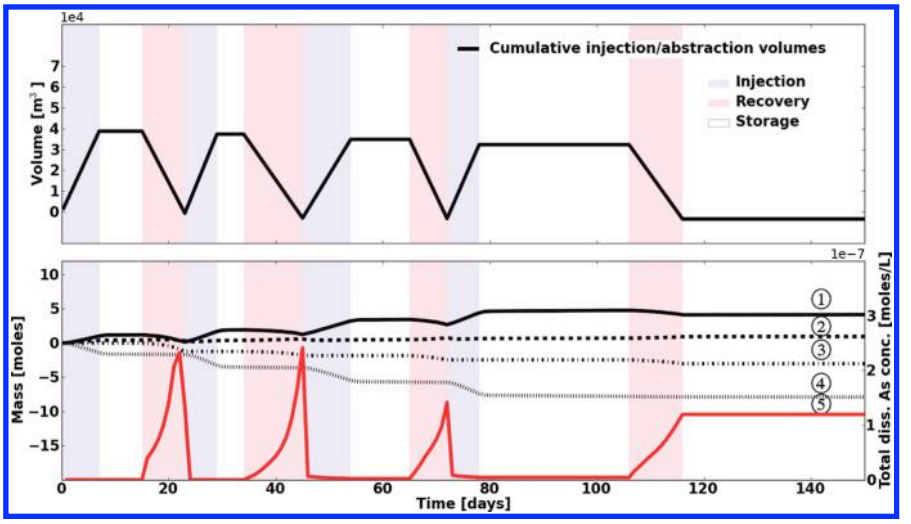

Figure 3. Temporal variation of the integrated mass of total dissolved and complexed arsenic in the aquifer, discharge of As from the ASR well, and As released from pyrite during oxidation for the first 4 ASR cycles. Simulated As concentrations are also shown as well as cumulative injection and abstraction volumes. 1: As complexed to HFO, 2: total dissolved As, 3: As discharged through well, 4: As mobilized through pyrite oxidation, 5: total dissolved As conc. at ASR well.

which occurred during this cycle, while measured ORP values remained consistently below 0 mV during all other ASR cycles. We speculate that oxygen may have been diluted during sample recovery due to mixing within the well with water received from the more reducing aquifer sections. In the initial periods of each simulated recovery phase the recovered water consisted mainly of the oxygen depleted injectate, followed by a period during which increasing proportions of even more reducing native groundwater migrated back toward the ASR well. During recovery $Fe(OH)_3$ was partially depleted as a result of its reductive dissolution. Where the dissolution upon contact with the anoxic groundwater occurred, ferrous iron was released (Figure 1). It then complexed with carbonates and precipitated as siderite. In model simulations that did not consider siderite precipitation dissolved iron concentrations were considerably overestimated compared to the measured concentrations (results not shown). Overall the calibrated reactive transport model reproduced closely the observed redox patterns in both the ASR and the observation well.

Analysis of Arsenic Fate. During the injection of aerated water, kinetically controlled oxidation of pyrite occurred where oxygen was not depleted. As was simultaneously released at a rate proportional to the simulated pyrite oxidation rate. The extent of the zone where pyrite oxidation and simultaneous As release occurred varied depending on aquifer transmissivity and pyrite content, i.e., over ~15 to 50 m at the end of the shorter injection cycles 1 to 4 (injected volume of $35-39 \times 10^6$ L/cycle) and over ~50 to 120 m at the end of the prolonged injection cycle 6. This is illustrated in Figure 2, which shows the simulated concentration profiles for oxygen and the corresponding simulated zone of pyrite oxidation for the high conductivity horizon. During injection, under predominantly oxic conditions the released As is transported as arsenate in radial direction away from the ASR well. Its migration, however, is strongly affected by sorption to HFO. This attenuation mechanism is effective in limiting the lateral migration of As and in maintaining dissolved As concentrations at a low level throughout the aquifer over the entire injection period. Over the duration of the 7 simulated ASR cycles, arsenic found in solution accounted on average for only 22% of the As released due to pyrite oxidation.

During the first and the following recovery phases, when the previously displaced anoxic native groundwater was drawn back toward the ASR well, the dissolution of HFO caused the release of sorbed As, mainly as arsenite, under the progressively more reducing conditions. This resulted in increased total As concentrations in the recovered water, as illustrated in Figure 3. The plots show the simulated cumulative As mass as well as dissolved As concentrations at the ASR well for the first 4 ASR cycles and provides a detailed assessment of As partitioning among mineral phases, surface complexes, and the aqueous phase and how the partitioning changes between injection, storage, and recovery. During each cycle As concentrations continued to rise at the ASR well until the end of recovery, i.e., the maximum As concentrations were attained at abstraction/injection ratios of close to 100% or above. A survey of 52 ASR wells[1] shows this to be a common response at As affected ASR sites. However, comparative simulations (not shown) suggest the timing of the As peak to be strongly related to the redox conditions of the native groundwater, i.e., the more reducing the ASR target aquifer, the faster HFO dissolves during recovery events with As peak concentrations attained at recovery/injection ratios below 100%, a trend also commonly reported from affected sites.[1]

The model simulations suggest that not all of the freshly accumulated HFO during injection phases became dissolved during recovery, except when abstraction volumes exceeded injected volumes. Subsequently, the total mass of HFO and, thus, the associated sorption capacity successively increased over time (Figure S6). This resulted in an increased attenuation of As due to sorption to (i) neo-formed HFO surfaces and (ii) to previously precipitated but not subsequently dissolved HFO surfaces (Figure 3). Therefore the ratio of As mass mobilized during injection and that discharged during recovery varied. At the end of the model simulation, i.e., the end of ASR cycle 7, when ~116% of the total injected water volume was recovered, over 70% (~48 mol) of the mobilized As mass was extracted. However, this amounts to only a small reduction of the total As mass prevailing in the target zone, as estimated based on the (initial) pyrite concentration. At the end of cycle 7, a predicted reduction of 6% of the total As mass occurred, from within a

radius of 1.5 m around the ASR well, declining to ~0.5% for a radial distance of 30 m (Figure S7). This implies that slow "As flushing" of the target zone via repeated ASR cycles is in principle possible but not very effective.

Transferability of Conceptual/Numerical Model to Other ASR Sites. The numerical model developed based on the data collected at the Bradenton site describes a system where oxic potable water is injected into an aquifer characterized by anoxic and brackish (TDS ~ 1200 mg L^{-1}) native conditions. While these conditions are comparable to many other ASR sites, particularly in Florida, differences in the quality of the injectate, the redox conditions, and salinity of the native groundwater will determine the extent to which the model is transferrable to other ASR operations. The most distinct differences are expected for sites where more nutrient and organic-rich, e.g., reclaimed water rather than drinking water is injected. Depending on the concentration and reactivity of the organic carbon, its presence will, besides pyrite oxidation, become an increasingly important driving force for geochemical changes. In this case more reducing conditions may develop within aquifer zones occupied by the injectate, thereby reducing As attenuation by sorption to HFO, compared to the present study site.

At those ASR sites where the native groundwater has higher TDS concentrations, physical and geochemical processes may differ, and density-driven flow patterns may develop[21] with associated impacts on arsenic breakthrough behavior. Second, As mobilization by desorption from HFO may become more important. While we conclude that destruction of sorption sites was the main As release mechanism at the Bradenton site, comparative simulations where HFO was not allowed to dissolve demonstrate that competitive displacement of As from sorption sites by other inorganic solutes is an equally effective As release mechanism (Figure S8). Model results suggest that the high alkalinity of the native groundwater compared to the injectate was thereby the major driving force for As displacement from HFO. The simulations imply that a displacement of the sorbed arsenic by the major anions contained in the relatively saline ambient water is sufficient to mobilize arsenic. Importantly, dissolution of HFO, while likely under the redox conditions observed at the Bradenton site, is not necessarily required to obtain elevated arsenic concentrations during recovery. It follows that arsenic remobilization will generally be the combined effect of (a) a reduction in sorptive capacity of As on HFO due to elevated TDS in the native groundwater and (b) reductive dissolution of HFO. Both models are not mutually exclusive and which one takes priority depends on the prevailing redox conditions and the salinity of the native groundwater.

Uncertainties. Despite the complexity of the model, several assumptions are likely to be substantial oversimplifications of the subsurface system. The dissolved As concentrations, which were reasonably well described for the Bradenton site, are strongly controlled by solubilities and mineral reaction rates of pyrite and HFO and by competing pH-dependent adsorption reactions. These processes and their respective parameters are highly nonlinear and will be affected by nonuniqueness and uncertainty, in particular where measured data were incomplete (e.g., NO_3, DOC, PO_4, microbial concentrations) or not available at the required density (H_2S, Fe^{2+}). Open bore construction and subsequent depth integrated sampling also contributed to the uncertainty in process/parameter identification. Future studies at other affected ASR sites with more detailed geochemical/hydrogeological data and multiple observation bores will provide additional constraints to test and improve our conceptual model. Despite these limitations, the present model is capable of providing valuable insights into the coupled flow and reaction patterns that affect arsenic fate during ASR of potable water. This quantification framework will provide a useful tool for the assessment and optimization of operational conditions and their impact on As mobility at affected sites.

■ ASSOCIATED CONTENT

Supporting Information. Additional information on operational conditions at the Bradenton ASR site, model set up, simulated breakthrough curves, and mass balances for arsenic and other selected species. This material is available free of charge via the Internet at http://pubs.acs.org.

■ AUTHOR INFORMATION

Corresponding Author
*Phone: +61-8-82012724. Fax: +61-8-82015635. E-mail: ilka.wallis@csiro.au.

■ ACKNOWLEDGMENT

We gratefully acknowledge Don Ellison (South West Florida Water Management District) and Rommy Lahera (FDEP Tampa) for providing geochemical data for the Bradenton ASR site. We also thank Janek Greskowiak for kindly providing valuable input and computational resources and Peter Dillon, Joanne Vanderzalm and Carlos Descourvieres for their reviews of earlier versions of the manuscript. The financial support provided by Land and Water Australia is gratefully acknowledged. Stuart Norton was supported in part by the Water Resources Research Center at the University of Florida, while Henning Prommer was supported by the Western Australian Water Foundation.

■ REFERENCES

(1) ASR Systems. In *Evaluation of Arsenic Mobilization Processes occuring during Aquifer Storage Recovery Activities*; District, S. F. W. M., Ed.; 2007.

(2) Stuyfzand, P. J. In *ASR Arsenic Surrogate Model;* District, , S. F. W. M., Ed.; 2008.

(3) Arthur, J. D.; Dabous, A. A.; Cowart, J. B. In *Mobilization of arsenic and other trace elements during aquifer storage and recovery, southwest Florida*; U.S. Geological Survey Artificial Recharge Workshop Sacramento, CA 2002; Aiken, G. R.; Kuniansky, E. L., Eds.; Sacramento, CA, 2002; pp 20−32.

(4) Appelo, C. A. J.; de Vet, W. W. J. M. Modeling in situ iron removal from groundwater with trace elements such as As. In *Arsenic in groundwater*; Welch, A. H., Stollenwerk, K. G., Eds.; Kluwer Academic: Boston, 2003; pp 381−401.

(5) Vanderzalm, J. L.; Dillon, P. J.; Barry, K. E.; Miotlinski, K.; Kirby, J. K.; Le Gal La Salle, C. Arsenic mobility under variable redox conditions induced during ASR. *Appl. Geochem.* accepted for publication.

(6) Stuyfzand, P. J.; Timmer, H. *Deep well injection at the Langerak and Nieuwegein sites in the Netherlands: chemical reactions and their modeling*; Kiwa-SWE 96.006; Nieuwegein, Netherlands, 1999.

(7) Wallis, I.; Prommer, H.; Simmons, C. T.; Post, V.; Stuyfzand, P. J. Evaluation of Conceptual and Numerical Models for Arsenic Mobilization and Attenuation during Managed Aquifer Recharge. *Environ. Sci. Technol.* **2010**, *44* (13), 5035–5041.

(8) Price, R. E.; Pichler, T. Abundance and mineralogical association of arsenic in the Suwannee Limestone (Florida): Implications for arsenic

release during water-rock interaction. *Chem. Geol.* **2006**, *228* (1−3), 44–56.

(9) Jones, G. W.; Pichler, T. Relationship between pyrite stability and arsenic mobility during aquifer storage and recovery in southwest central Florida. *Environ. Sci. Technol.* **2007**, *41* (3), 723–730.

(10) Mirecki, J. E. *Geochemical Models of Water-Quality Chnages During Aquifer Storage Recovery (ASR) Cycle Tests, Phase I: Geochemical Models Using Existing Data*; U.S. Army Corps of Engineers: Vicksburg, 2006.

(11) Norton, S. B. *Quantifying the near-borehole geochemical response during Aquifer Storage and Recovery: Application of "Push-Pull" analytical techniques to ASR cycle testing*; University of Florida, 2007.

(12) Arthur, J. D. C., B., J.; Dabous, A. A. Florida Aquifer Storage and Recovery Geochemical Study: Year Three Progress Report. In *Open File Report 83*; Protection, , D. o. E., Ed.; Florida Geological Survey: Tallahassee, 2001.

(13) Prommer, H.; Barry, D. A.; Zheng, C. MODFLOW/MT3DMS-Based Reactive Multicomponent Transport Modeling. *Groundwater* **2003**, *41* (2), 247–257.

(14) Prommer, H.; Stuyfzand, P. J. Identification of temperature-dependent water quality changes during a deep well injection experiment in a pyritic aquifer. *Environ. Sci. Technol.* **2005**, *39* (7), 2200–2209.

(15) Greskowiak, J.; Prommer, H.; Vanderzalm, J.; Pavelic, P.; Dillon, P., Modeling of carbon cycling and biogeochemical changes during injection and recovery of reclaimed water at Bolivar, South Australia. *Water Resour. Res.* **2005**, *41*, (10).

(16) Williamson, M. A.; Rimstidt, J. D. The Kinetics and Electrochemical Rate-Determining Step of Aqueous Pyrite Oxidation. *Geochim. Cosmochim. Acta* **1994**, *58* (24), 5443–5454.

(17) Descourvieres, C.; Prommer, H.; Oldham, C.; Greskowiak, J.; Hartog, N. Kinetic Reaction Modeling Framework for Identifying and Quantifying Reductant Reactivity in Heterogeneous Aquifer Sediments. *Environ. Sci. Technol.* **2010**, *44*, 6698–6705.

(18) Dzombak, D. A.; Morel, F. M. M. *Surface Complexation Modeling*; Wiley and Sons: New York, 1990.

(19) Appelo, C. A. J.; Van der Weiden, M. J. J.; Tournassat, C.; Charlet, L. Surface complexation of ferrous iron and carbonate on ferrihydrite and the mobilization of arsenic. *Environ. Sci. Technol.* **2002**, *36* (14), 3096–3103.

(20) Appelo, C. A. J.; Drijver, B.; Hekkenberg, R.; de Jonge, M. Modeling in situ iron removal from ground water. *Ground Water* **1999**, *37* (6), 811–817.

(21) Ward, J. D.; Simmons, C. T.; Dillon, P. J. A theoretical analysis of mixed convection in aquifer storage and recovery: How important are density effects? *J. Hydrol.* **2007**, *343* (3−4), 169–186.